

Spectral and Energy Efficiency Tradeoff for Pinching-Antenna Systems

Zihao Zhou, Zhaolin Wang, *Member, IEEE*, and Yuanwei Liu, *Fellow, IEEE*

Abstract—The joint transmit and pinching beamforming design for spectral efficiency (SE) and energy efficiency (EE) tradeoff in pinching-antenna systems (PASS) is proposed. Both PASS-enabled single- and multi-user communications are considered. In the single-user scenario, it is proved that the optimal pinching antenna (PA) positions are independent of the transmit beamforming. Based on this insight, a two-stage joint beamforming design is proposed. Specifically, in the first stage, an iterative closed-form refinement (ICR) scheme is proposed to align the phases of the received signals, based on which a PA placement framework is proposed. In the second stage, the closed-form solution for the optimal transmit beamformer is derived given the optimal PA positions. In the multi-user scenario, an alternating optimization (AO)-based joint beamforming design is proposed to balance the SE-EE performance while taking the quality-of-service (QoS) requirements into account. It is proved that the proposed AO-based algorithm is guaranteed to converge when no constraints are violated in PA placement subproblem. Numerical results demonstrate that: 1) the proposed algorithms significantly improve joint SE-EE performance with fast convergence speed; 2) the SE-EE tradeoff regime gap between PASS and conventional multi-antenna system widens as the number of PAs and service coverage increase.

Index Terms—Beamforming, energy efficiency, pinching-antenna systems, spectral efficiency.

I. INTRODUCTION

THE pursuit of higher capacity and efficiency has long been a consistent goal in wireless communication systems [1]. Over the past few decades, guided by the Shannon formula, researchers have optimized the systems by focusing on bandwidth [2], transmit power [3], and even the noise [4], while treating the wireless channel as a fixed system parameter. In recent years, however, the emergence of flexible-antenna techniques, such as reconfigurable intelligent surfaces (RISs) [5], fluid-antennas [6] and movable-antennas [7] has unlocked new possibilities for the design of wireless communication systems by treating the wireless channel itself as a reconfigurable parameter. Specifically, RISs modify the channel via programmable phase shifters, whereas fluid- and movable-antenna systems physically adjust the position of antenna elements to establish favorable channel conditions [8]. More importantly, flexible-antenna techniques are inherently compatible with multiple-input multiple-output (MIMO), a technology that has been among the most celebrated ones over the past thirty years. In particular, they introduce a new layer of electromagnetic beamforming through antenna reconfigurability within the MIMO architecture [9]. This in-

trinsic compatibility undoubtedly injects strong vitality into the development of flexible-antenna techniques.

Despite recent advances, the existing flexible-antenna techniques face inherent limitations, which may hinder their further application. Firstly, they exhibit insufficient capacities against large-scale fading. For instance, RIS introduces two separate links: the transmitter-to-RIS link and the RIS-to-receiver link. The increased propagation distance leads to more severe path loss [10]. While for fluid/movable antennas, the movement of antenna elements is constrained to the wavelength scale [11], which typically has an insignificant impact on large-scale fading. Secondly, for the flexible-antenna systems mentioned above, once deployed, it is difficult to change the number of antenna elements anymore, which means that the array size cannot be adaptively modified according to different user demands. This reflects the “inflexibility” of the existing flexible-antenna systems.

To address the aforementioned challenges, pinching-antenna system (PASS) emerges as a novel flexible-antenna technique to overcome large-scale fading while offering “ultraflexibility”. The concept of PASS and the experimental demonstrations were first given by NTT DOCOMO [12]. Specifically, PASS consists of one or more dielectric waveguides as transmission medium. By deploying multiple small, separated dielectric elements, referred to as *pinching antenna* (PA), onto the waveguides, the in-waveguide radio waves can be radiated into free space via these PAs. Unlike traditional flexible-antenna systems, PASS distinguishes itself by “ultraflexibility”, which mainly includes two aspects: 1) PASS overcomes the restriction that antenna movement can only be limited to the wavelength scale. Specifically, with the aid of waveguides which span across several to tens of meters [8], PAs can be deployed close to users, substantially reducing large-scale path loss and alleviating blockage from obstacles. Moreover, by jointly optimizing the placement of multiple PAs, a new capability, which is referred to as *pinching beamforming*, is enabled to further enhance signal quality; 2) by simply attaching additional PAs or releasing existing ones, changing the array size in PASS becomes extremely straightforward, which can well support the on-demand deployment.

These advantages aforementioned have spurred growing interest in investigating PASS from the perspectives of theoretical analysis and system optimization. Specifically, the authors of [10] presented the first comprehensive theoretical analysis for PASS in terms of ergodic sum rate. In [13], the closed-form expressions for the outage probability and average rate of PASS were derived. The authors of [14] investigated PASS from the perspective of array gain where the closed-form upper

The authors are with the Department of Electrical and Electronic Engineering, The University of Hong Kong, Hong Kong (e-mail: eezihaozhou@connect.hku.hk, zhaolin.wang@hku.hk, yuanwei@hku.hk)

bound on the array gain is derived, unveiling the optimal number of PAs and spacing. Considering PASS-assisted uplink communication system, the closed-form expressions for analytical, asymptotic and approximated ergodic rate were derived in [15]. In [16], the optimal position of PA was given under the user-fairness-oriented orthogonal multiple access (OMA) based communication. Furthermore, a growing body of recent literature is devoted to the performance analysis of PASS in combination with various other emerging technologies, such as simultaneous wireless information and power transfer (SWIPT) [17], integrated sensing and communications (ISAC) [18] and non-orthogonal multiple access (NOMA) [19].

In addition to performance analysis, researchers have also focused on optimizing the performance of PASS-assisted wireless communication systems in more general settings. For the single-waveguide employment, the authors of [11], proposed a two-stage algorithm to optimize the positions of PAs with the aim at maximizing the rate of the user. The sum rate maximization problem was investigated in PASS-assisted NOMA systems in [20]–[22]. Consider discrete PAs' positions, the authors of [23] investigated how many and at which positions the PAs need to be activated such that the sum rate is maximized. Also focusing on sum rate maximization, the authors of [24] addressed this problem in PASS-assisted uplink multiuser multiple-input single-output (MISO) systems. In [25], the sum rate was maximized by jointly optimizing the resource allocation and PAs' positions in a PASS-assisted wireless powered communication network (WPCN). In [26], a novel concept of waveguide division multiple access (WDMA) was proposed, and the power allocation as well as the pinching beamforming were jointly designed to maximize the sum rate.

Apart from the aforementioned works focusing on spectral efficiency (SE) optimization [11], [20]–[26], there have been other studies investigating the energy efficiency (EE) of PASS, which is an important metric that takes into account both system power consumption and throughput. For example, in [27], a NOMA-assisted uplink single-waveguide PASS was investigated, with the objective to maximize the EE by jointly optimizing the users' transmit power and the positions of PAs. The authors of [28] shifted the attention to downlink scenarios in a PASS assisted time-division multiple access (TDMA)-based system by jointly optimizing the transmit power, time allocation, as well as the positions of PAs under the quality-of-service (QoS) constraint.

While the work introduced above demonstrates the effectiveness of PASS in enhancing both SE and EE, they have predominantly focused on the optimization of either SE or EE. However, the objectives of maximizing SE and EE do not always coincide. On the contrary, they sometimes conflict, especially in moderate and high signal-to-noise ratio (SNR) regimes [29]. It is therefore essential to analyze and optimize the SE-EE trade-off for PASS, which is a critical aspect that remains largely unexplored. The main contributions are summarized as follows:

- We investigate the SE-EE trade-off for PASS, both in single- and multi-user scenarios. A transmit and pinching beamforming optimization problem is formulated to maximize the joint SE-EE performance while satisfying

the QoS requirements, transmit power budget, and positions constraints of PAs. Unlike conventional SE or EE-targeted design for PASS, our approach offers a generic framework to strike a balance between SE and EE, which provides guidance for configuring PASS flexibly.

- For single-user scenario, we prove that the optimal PA positions are independent of the transmit beamforming. Based on this insight, an efficient two-stage joint beamforming design is proposed: in the first stage, an iterative closed-form refinement (ICR) scheme is proposed to align the phases of the received signals, based on which a PA placement framework is proposed; In the second stage, under maximum ratio transmission (MRT), a closed-form solution is derived for the optimal transmit power with the given optimized PA positions.
- For multi-user scenario, an alternating optimization (AO) framework is proposed to address the joint SE-EE maximization problem. Using zero-forcing (ZF) beamforming, the optimization of transmit beamformer reduces to the design of a diagonal scalar power control matrix, which is optimized by deriving the convex upper bounds of the constraints. Meanwhile, the pinching beamforming is optimized by element-wise sequential partial swarm optimization (PSO) method. Furthermore, we prove that the proposed AO-based algorithm is guaranteed to converge when no constraints are violated in PA placement subproblem.
- Extensive numerical results validate the effectiveness of the proposed algorithms. The results demonstrate that: 1) the proposed algorithm significantly improve both SE and EE performance with fast convergence speed; 2) the SE-EE trade-off regime gap between PASS and conventional multiple-input multiple-output (MIMO) system widens when the number of PAs and spatial coverage increase, and PASS presents superior robustness across different service coverage. These results confirm the scalability and potential of PASS for communication systems.

The rest of this paper is structured as follows. In Section II, a joint SE-EE design in PASS-enabled single-user scenario is investigated. In Section III, the transmit and pinching beamforming are optimized in the multi-user scenario. Numerical results are provided in Section IV, which is followed by our conclusions in Section V.

Notations: Scalars, vectors, and matrices are represented by regular, bold lowercase, and bold uppercase (e.g., x , \mathbf{x} and \mathbf{X}) letters, respectively. The set of complex and real numbers are denoted by \mathbb{C} and \mathbb{R} , respectively. The inverse, transpose, conjugate transpose, and trace operators are denoted by $(\cdot)^{-1}$, $(\cdot)^T$, $(\cdot)^H$, and $\text{tr}(\cdot)$, respectively. The absolute value and Euclidean norm are denoted by $|\cdot|$ and $\|\cdot\|$, respectively. $\mathcal{CN}(a, b^2)$ is denoted as a circularly symmetric complex Gaussian distribution with mean a and variance b^2 . The expectation operator is denoted by $\mathbb{E}[\cdot]$.

II. JOINT SE-EE DESIGN FOR SINGLE-USER PASS

A. System Model

We first focus on a single-user downlink PASS as illustrated in Fig. 1. A single-antenna user is randomly located in a region

of size $D = D_x \times D_y$ m², with its position being specified as $\psi^u = [x^u, y^u, 0]^T$. A base station (BS) is equipped with M dielectric waveguides, each is attached with N pinching antennas (PAs), to simultaneously support this user. We assume that the waveguides are deployed along the x -axis at an altitude of h , and arranged in an array along the y -axis, with inter-waveguide spacing $d_y = D_y/(M-1)$ m. Let \mathcal{M} denotes the set of waveguides, and \mathcal{N}_m the set of PAs mounted on the m -th waveguide. Each waveguide is fed by a dedicated radio frequency (RF) chain located at $\alpha_{m,0} = [-D_x/2, y_m, h]^T$ for $m \in \mathcal{M}$. The position of the n -th PA on the m -th waveguide is given by $\alpha_{m,n} = [x_{m,n}^p, y_m, h]^T$ for $m \in \mathcal{M}$ and $n \in \mathcal{N}_m$. The x -axis coordinates of all PAs can be stacked into a matrix $\mathbf{X} = [\mathbf{x}_1, \mathbf{x}_2, \dots, \mathbf{x}_M] \in \mathbb{R}^{N \times M}$, where $\mathbf{x}_m = [x_{m,1}^p, x_{m,2}^p, \dots, x_{m,N}^p]^T \in \mathbb{R}^{N \times 1}$ represents the x -axis coordinate vector of PAs on the m -th waveguide. In this work, \mathbf{X} is treated as a key optimization variable for the design of pinching beamforming.

In PASS, the end-to-end channel from the BS to ground user consists of two components: *in-waveguide propagation* and *free-space propagation* [30], as shown in Fig. 1. For the in-waveguide propagation, the signal emitted from each PA on the same waveguide can be regarded as a phase-shifted version of that at the feed point of the waveguide. The in-waveguide channel vector for the m -th waveguide can be expressed as

$$\mathbf{g}_m(\mathbf{x}_m) = \left[e^{-j\frac{2\pi}{\lambda_g} \|\alpha_{m,0} - \alpha_{m,1}\|}, \dots, e^{-j\frac{2\pi}{\lambda_g} \|\alpha_{m,0} - \alpha_{m,N}\|} \right], \quad (1)$$

where $\lambda_g = \lambda/n_{\text{eff}}$ denotes the guided wavelength with λ and n_{eff} being the free-space wavelength and the waveguide effective refractive index, respectively. Therefore, the overall in-waveguide channel matrix can be defined by block-diagonal matrix $\mathbf{G}(\mathbf{X}) \in \mathbb{C}^{MN \times N}$, which is given as

$$\mathbf{G}(\mathbf{X}) = \text{blkdiag} \{ \mathbf{g}_1(\mathbf{x}_1), \dots, \mathbf{g}_M(\mathbf{x}_M) \}. \quad (2)$$

For free-space propagation, the classical indoor scenarios is considered where the user is in line-of-sight (LoS) with the PAs [31]. The free-space channel vector from the m -th waveguide to the user can be written as

$$\mathbf{h}_m^H(\mathbf{x}_m) = \left[\frac{\sqrt{\eta} e^{-j\frac{2\pi}{\lambda} \|\psi^u - \alpha_{m,1}\|}}{\|\psi^u - \alpha_{m,1}\|}, \dots, \frac{\sqrt{\eta} e^{-j\frac{2\pi}{\lambda} \|\psi^u - \alpha_{m,N}\|}}{\|\psi^u - \alpha_{m,N}\|} \right], \quad (3)$$

where $\eta = c^2/(16\pi^2 f_c^2)$ is a constant with c and f_c being the speed of light and the carrier frequency, respectively. $\|\psi^u - \alpha_{m,n}\|$ represents the distance between the n -th PA on the m -th waveguide and the user, which is computed by $\|\psi^u - \alpha_{m,n}\| = \sqrt{(x^u - x_{m,n}^p)^2 + (y^u - y_m)^2 + h^2}$. Thus, the overall free-space channel vector $\mathbf{h}^H(\mathbf{X}) \in \mathbb{C}^{1 \times MN}$ is given as follows:

$$\mathbf{h}^H(\mathbf{X}) = \left[\mathbf{h}_1^H(\mathbf{x}_1), \mathbf{h}_2^H(\mathbf{x}_2), \dots, \mathbf{h}_M^H(\mathbf{x}_M) \right]. \quad (4)$$

Let $s \in \mathbb{C}$ and $\mathbf{w} \in \mathbb{C}^{M \times 1}$ denote the transmitted signal with $\mathbb{E}[|s|^2] = 1$ and digital beamforming vector, respectively. Therefore, the received signal at the user can be expressed as

$$y = \mathbf{h}^H(\mathbf{X}) \mathbf{G}(\mathbf{X}) \mathbf{w} s + z, \quad (5)$$

where $z \sim \mathcal{CN}(0, \sigma^2)$ denotes the additive white Gaussian noise (AWGN) with a power of σ^2 . Thus, the SNR is given as $\gamma = \frac{|\mathbf{h}^H(\mathbf{X}) \mathbf{G}(\mathbf{X}) \mathbf{w}|^2}{\sigma^2}$. According to [29], the SE f_{SE} and EE

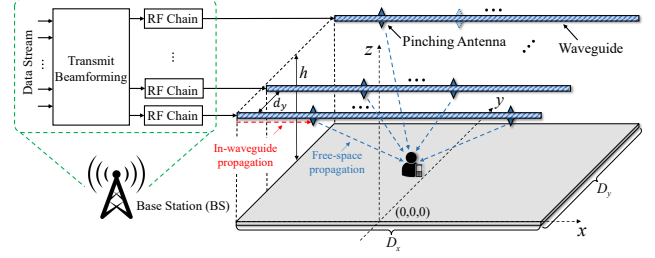


Fig. 1. System model for PASS-enabled single-user communications.

f_{EE} for the considered scenario is defined as

$$\begin{cases} f_{\text{SE}}(\mathbf{w}, \mathbf{X}) = \log_2(1 + \gamma) \\ f_{\text{EE}}(\mathbf{w}, \mathbf{X}) = \frac{f_{\text{SE}}(\mathbf{w}, \mathbf{X})}{\|\mathbf{w}\|^2 + P_f + \chi f_{\text{SE}}(\mathbf{w}, \mathbf{X})} \end{cases} \quad (6)$$

where $\|\mathbf{w}\|^2$ represents the transmit power consumption, P_f and $\chi \geq 0$ denote the aggregate fixed circuit power of the system and a constant demonstrating the coding, decoding, and backhaul power consumption per unit data rate (W/(bit/s/Hz)), respectively.

B. Problem Formulation

We aim to balance the SE and EE performance of PASS by jointly optimizing the transmit and pinching beamforming. The resulting multi-objective optimization (MOO) problem incorporates two conflicting performance metrics, i.e., SE and EE. The weighted product method is adopted to convert the MOO problem into a single-objective optimization (SOO) problem as follows:¹

$$(\mathbf{P1-1}) : \max_{\mathbf{w}, \mathbf{X}} [f_{\text{SE}}(\mathbf{w}, \mathbf{X})]^\beta \times [f_{\text{EE}}(\mathbf{w}, \mathbf{X})]^{1-\beta} \quad (7a)$$

$$\text{s.t. } x_{m,n}^p \in [0, D_x], \forall m, \forall n, \quad (7b)$$

$$|x_{m,n}^p - x_{m,n-1}^p| \geq \Delta_{\min}, \forall m, \forall n, \quad (7c)$$

$$\|\mathbf{w}\|^2 \leq P_T, \quad (7d)$$

where constraint (7b) ensures that each PA is positioned within the valid range of the waveguide, Δ_{\min} in (7c) is the minimum spacing required to prevent mutual coupling between the PAs [33], and (7d) refers to the constraint on transmit power at the BS side. Noted that problem (P1-1) is non-convex since \mathbf{w} and \mathbf{X} are strongly coupled in (7a). Fortunately, for any given PA positions \mathbf{X} , the optimal transmit beamforming \mathbf{w}^* of (P1-1) can be obtained by using MRT strategy:

$$\mathbf{w}^* = \sqrt{P} \frac{(\mathbf{h}^H(\mathbf{X}) \mathbf{G}(\mathbf{X}))^H}{\|\mathbf{h}^H(\mathbf{X}) \mathbf{G}(\mathbf{X}) \mathbf{w}\|}, \quad (8)$$

where P is the scalar transmit power. Therefore, the SNR for the user under MRT strategy can be given by $\gamma = P \|\mathbf{h}^H(\mathbf{X}) \mathbf{G}(\mathbf{X})\|^2 / \sigma^2$. Accordingly, the SE and EE can be rewritten as

$$\begin{cases} f_{\text{SE}}(P, \mathbf{X}) = \log_2(1 + \gamma), \\ f_{\text{EE}}(P, \mathbf{X}) = \frac{f_{\text{SE}}(P, \mathbf{X})}{P + P_f + \chi f_{\text{SE}}(P, \mathbf{X})}. \end{cases} \quad (9)$$

¹Unlike conventional weighted-sum method, weighted-product method avoids scalarization of objective functions, which can help simplify the analysis [32].

Based on the above transformation, the optimization of the digital beamforming vector reduces to the design of the scalar transmit power P . In the following, we first optimize one variable by fixing the other, and then a two-stage optimization framework is demonstrated.

C. Optimization of PA Positions

To facilitate the optimization of PA positions, we first transform problem **(P1-1)** into the following equivalent form for a given P :

$$\text{(P1-2)} : \max_{\mathbf{X}} \beta \ln f_{\text{SE}}(\mathbf{X}) + (1 - \beta) \ln f_{\text{EE}}(\mathbf{X}) \text{ s.t. (7b), (7c)} \quad (10)$$

Lemma 1. The objective function of problem **(P1-2)** is strictly increasing with $f_{\text{SE}}(\mathbf{X})$.

Proof: Let f denote the objective function in **(P1-2)** and take the first derivative of f with respect to $f_{\text{SE}}(\mathbf{X})$ leads to

$$f' = \frac{\beta}{f_{\text{SE}}(\mathbf{X})} + \frac{1 - \beta}{f_{\text{EE}}(\mathbf{X})} \frac{P + P_f}{(P + P_f + \chi f_{\text{SE}}(\mathbf{X}))^2}, \quad (11)$$

it is clear that $f' > 0$, so f is increasing with $f_{\text{SE}}(\mathbf{X})$. The proof is thus completed. \blacksquare

Based on **Lemma 1**, problem **(P1-2)** is equivalent to a SE-maximization problem, which can be formulated as

$$\text{(P1-3)} : \max_{\mathbf{X}} \log_2 (1 + \gamma) \text{ s.t. (7b), (7c).} \quad (12)$$

From problem **(P1-3)**, it is noticed that maximizing the SE is equivalent to maximizing the SNR. Therefore, problem **(P1-3)** can be equivalently recast as follows:

$$\text{(P1-4)} : \max_{\mathbf{X}} \left| \sum_{m=1}^M \sum_{n=1}^N \frac{e^{-j\phi_{m,n}}}{\|\boldsymbol{\alpha}_{m,n} - \boldsymbol{\psi}^u\|} \right| \quad (13a)$$

$$\text{s.t. (7b), (7c),} \quad (13b)$$

$$\phi_{m,n} = \frac{2\pi}{\lambda} \|\boldsymbol{\alpha}_{m,n} - \boldsymbol{\psi}^u\| + \frac{2\pi}{\lambda_g} \|\boldsymbol{\alpha}_{m,0} - \boldsymbol{\alpha}_{m,n}\|. \quad (13c)$$

The objective function in **(P1-4)** reveals that the placement of PAs affects both large-scale path loss and the phase shifts. Based on [11], the optimal position of the n -th PA on the m -th waveguide that maximizes the summation of reciprocals of distances can be obtained as

$$\boldsymbol{\alpha}_{m,n}^{\text{opt}} = \left[x^u - \left(\frac{N-1}{2} - (n-1) \right) \Delta_{\min}, y_m, h \right], \forall m, n. \quad (14)$$

It should be noted that the PA positions obtained from eq. (14) are coarse, and further refinement is needed to ensure constructive signal combination at the user. Unlike [11] that adopts discrete point searching which yields sub-optimal solution, this paper proposes an iterative closed-form refinement (ICR) scheme, based on which a PA placement framework for more general multi-waveguide scenario is developed. We will introduce separately in two cases below.

1) *Refine on A Single Waveguide:* We first optimize the placement of PAs in the direction of the positive half of the x -axis. For the m -th waveguide, the x -axis coordinate of the n -th PA is initialized as $x_{m,n-1}^p + \Delta_{\min}$ based on (14). However, this solution does not necessarily maximize the user's received signal strength. Therefore, the position of $x_{m,n}^p$ should be adjusted by adding a positive offset Δ' . In this case, according

to the condition of phase alignment $\phi_{m,n} - \phi_{m,n-1} = 2k\pi$, optimizing $x_{m,n}^p$ is equivalent to finding a Δ' such that the following equation holds:

$$\begin{aligned} & \frac{2\pi}{\lambda} \left(\sqrt{(x_{m,n-1}^p + \Delta_{\min} + \Delta' - x^u)^2 + A_1} - \|\boldsymbol{\alpha}_{m,n-1}^{\text{opt}} - \boldsymbol{\psi}^u\| \right) \\ & + \frac{2\pi}{\lambda_g} (x_{m,n-1}^p + \Delta_{\min} + \Delta' - x_{m,n-1}^{p,\text{opt}}) = 2k\pi, \end{aligned} \quad (15)$$

where $A_1 = (y_m - y^u)^2 + h^2$, $\boldsymbol{\alpha}_{m,n-1}^{\text{opt}}$ denotes the position of the $(n-1)$ -th PA on the m -th waveguide after refining, while $x_{m,n-1}^{p,\text{opt}}$ represents its corresponding x -axis coordinate, and k is an integer. By transposition and rearrangement, (15) can be expressed in the standard form of a quadratic equation: $a_1(\Delta')^2 + b_1\Delta' + c_1 = 0$, and its solution can be readily obtained when $b_1^2 - 4a_1c_1 \geq 0$:

$$\Delta' = \frac{-b_1 \pm \sqrt{b_1^2 - 4a_1c_1}}{2a_1}, \quad (16)$$

the coefficients a_1 , b_1 , and c_1 in (16) are given by

$$\begin{cases} a_1 = 1 - (\lambda/\lambda_g)^2, \\ b_1 = 2(x_{m,n-1}^p + \Delta_{\min} - x^u) + 2\lambda(k\lambda + \|\boldsymbol{\alpha}_{m,n-1}^{\text{opt}} - \boldsymbol{\psi}^u\| - \lambda(x_{m,n-1}^p + \Delta_{\min} - x_{m,n-1}^{p,\text{opt}})/\lambda_g)/\lambda_g, \\ c_1 = (x_{m,n-1}^p + \Delta_{\min} - x^u)^2 + (y_m - y^u)^2 + h^2 \\ \quad - (k\lambda + \|\boldsymbol{\alpha}_{m,n-1}^{\text{opt}} - \boldsymbol{\psi}^u\| - \lambda(x_{m,n-1}^p + \Delta_{\min} - x_{m,n-1}^{p,\text{opt}})/\lambda_g)^2. \end{cases} \quad (17)$$

It should be noted that a valid solution Δ' must satisfy: 1) $\Delta' \geq 0$; 2) $k\lambda + \|\boldsymbol{\alpha}_{m,n-1}^{\text{opt}} - \boldsymbol{\psi}^u\| - \lambda(x_{m,n-1}^p + \Delta_{\min} - x_{m,n-1}^{p,\text{opt}})/\lambda_g - \lambda\Delta'/\lambda_g \geq 0$. If the two roots both satisfy the two conditions, we keep the smallest one as the final solution.

For the position refining of PAs in the direction of the negative half of the x -axis, the procedure remains identical to that described above, the only difference is the solved equation becomes:

$$\begin{aligned} & \frac{2\pi}{\lambda} \left(\|\boldsymbol{\alpha}_{m,n+1}^{\text{opt}} - \boldsymbol{\psi}^u\| - \sqrt{(x_{m,n+1}^p - \Delta_{\min} - \Delta' - x^u)^2 + A_1} \right) \\ & + \frac{2\pi}{\lambda_g} (x_{m,n+1}^{p,\text{opt}} - (x_{m,n+1}^p - \Delta_{\min} - \Delta')) = 2k\pi. \end{aligned} \quad (18)$$

When $b_2^2 - 4a_2c_2 \geq 0$, the solution of (18) can be given as

$$\Delta' = \frac{-b_2 \pm \sqrt{b_2^2 - 4a_2c_2}}{2a_2}, \quad (19)$$

where the coefficients a_2 , b_2 , and c_2 are given by

$$\begin{cases} a_2 = 1 - (\lambda/\lambda_g)^2, \\ b_2 = -2(x_{m,n+1}^p - \Delta_{\min} - x^u) - 2\lambda(\|\boldsymbol{\alpha}_{m,n+1}^{\text{opt}} - \boldsymbol{\psi}^u\| - k\lambda + \lambda(x_{m,n+1}^p - x_{m,n+1}^{p,\text{opt}} + \Delta_{\min})/\lambda_g), \\ c_2 = (x_{m,n+1}^p - \Delta_{\min} - x^u)^2 + (y_m - y^u)^2 + h^2 \\ \quad - (\|\boldsymbol{\alpha}_{m,n+1}^{\text{opt}} - \boldsymbol{\psi}^u\| - k\lambda + \lambda(x_{m,n+1}^p - x_{m,n+1}^{p,\text{opt}} + \Delta_{\min})/\lambda_g)^2. \end{cases} \quad (20)$$

For a valid solution Δ' , the following two conditions must be satisfied: 1) $\Delta' \geq 0$; 2) $\|\boldsymbol{\alpha}_{m,n+1}^{\text{opt}} - \boldsymbol{\psi}^u\| - k\lambda + \lambda(x_{m,n+1}^p - x_{m,n+1}^{p,\text{opt}} + \Delta_{\min})/\lambda_g + \lambda\Delta'/\lambda_g \geq 0$.

2) *Refine Across Multiple Waveguides:* To refine the PA positions on a single waveguide, a *reference PA* is first selected, and the phase shift corresponding to this reference

Algorithm 1 The proposed ICR scheme

```

1: Initialize: The position of next or previous PA, the user
   location  $\psi^u$ , set  $k = 1$ 
2: repeat
3:   if  $b_i^2 - 4a_i c_i \geq 0$ ,  $i \in \{1, 2, 3\}$  then
4:     Get the solutions by eq. (15), (18) or (21) according
       to the value of  $i$ .
5:   if at least one solution is valid then
6:     Get the minimum valid solution.
7:   Break.
8:   else
9:      $k = k + 1$ .
10:  end if
11:  else
12:     $k = k + 1$ .
13:  end if
14: until a valid solution is found

```

PA is used to optimize the positions of other PAs. According to [11], this reference PA is the $(N+1)/2$ -th (if N is odd) or the $N/2$ -th PA (if N is even) on the first waveguide. However, for the m -th waveguide ($m > 1$), all PA positions require refinement. Here, we describe the refinement of its central PA² on this m -th waveguide; adjustments to the remaining PAs on this waveguide follow the method introduced in the previous part. Thus, when $m > 1$, we consider solving the following equation:

$$\frac{2\pi}{\lambda} \left(\sqrt{(x_{m, \{\frac{N+1}{2}, \frac{N}{2}\}}^p + \Delta' - x^u)^2 + A_1} - C_3 \right) \frac{2\pi}{\lambda_g} \Delta' = 2k\pi, \quad (21)$$

where $C_3 = \|\alpha_{1, \{\frac{N+1}{2}, \frac{N}{2}\}}^{\text{opt}} - \psi^u\|$. When $b_3^2 - 4a_3 c_3 \geq 0$, the solution of (21) can be given as

$$\Delta' = \frac{-b_3 \pm \sqrt{b_3^2 - 4a_3 c_3}}{2a_3}, \quad (22)$$

where the coefficients a_3 , b_3 , and c_3 are given by

$$\begin{cases} a_3 = 1 - (\lambda/\lambda_g)^2, \\ b_3 = 2(x_{m, \{\frac{N+1}{2}, \frac{N}{2}\}}^p - x^u) + 2\lambda(k\lambda + \|\alpha_{1, \{\frac{N+1}{2}, \frac{N}{2}\}}^{\text{opt}} - \psi^u\|)/\lambda_g, \\ c_3 = (x_{m, \{\frac{N+1}{2}, \frac{N}{2}\}}^p - x^u)^2 + (y_m - y^u)^2 + h^2 \\ \quad - (k\lambda + \|\alpha_{1, \{\frac{N+1}{2}, \frac{N}{2}\}}^{\text{opt}} - \psi^u\|)^2, \end{cases} \quad (23)$$

A valid solution Δ' of (21) must satisfy: 1) $\Delta' \geq 0$; 2) $k\lambda + \|\alpha_{1, \{\frac{N+1}{2}, \frac{N}{2}\}}^{\text{opt}} - \psi^u\| - \lambda\Delta'/\lambda_g \geq 0$.

From (15), (18), and (21), we note that k is a variable whose value may influence the existence of a solution to the equations. Therefore, the core idea of ICR is to solve the equation starting from $k = 1$. If no valid solution is found, k is incremented by 1 until a valid solution is obtained. The procedure of ICR is summarized in **Algorithm 1**.

Theorem 1. **Algorithm 1** is guaranteed to find a valid solution within a finite number of iterations.

Proof: According to our definition of position offset Δ' , we have $\Delta' \geq 0$. Therefore, being able to find a valid solution

²The central PA is the $(N+1)/2$ -th or the $N/2$ -th PA according to the parity of N .

Algorithm 2 The proposed PA placement framework

```

1: Initialize: The rough positions of PAs based on eq. (14),
   the user location  $\psi^u$ .
2: Get the rough position of the  $(N+1)/2$ -th or  $N/2$ -th PA
   on the first waveguide.
3: for  $m = 1$  to  $M$  do
4:   for  $n = \{\frac{N+1}{2} + 1$  or  $\frac{N}{2} + 1\}$  to  $N$  do
5:     Get the refined position of PA using Algorithm 1.
6:   end for
7:   for  $n = \{\frac{N+1}{2} - 1$  or  $\frac{N}{2} - 1\}$  down to 1 do
8:     Get the refined position of PA using Algorithm 1.
9:   end for
10:  if  $m < M$  then
11:    Get the refined position of the  $\frac{N+1}{2}$ -th or  $\frac{N}{2}$ -th PA
        on the  $(m+1)$ -th waveguide based on Algorithm 1.
12:  end if
13: end for

```

implies that the left-hand sides of eq. (15), (18) and (21) must necessarily intersect with $2k\pi$ within the range $[0, +\infty)$, where k is a finite value. Noting that the left-hand sides of eq. (15), (18) and (21) are continuous functions in $[0, +\infty)$, it follows that they are bounded on the interval $[0, +\infty)$, which implies that k is bounded. The proof is thus completed. ■

In simulation, a valid solution is typically found with a small k , ensuring fast ICR execution. Based on ICR, the overall PA placement framework is summarized in **Algorithm 2**.

D. Optimization of Transmit Power

In this subsection, we focus on the optimization of transmit power P at BS given fixed PA positions \mathbf{X} . By defining $\zeta = \|\mathbf{h}^H(\mathbf{X})\mathbf{G}(\mathbf{X})\|^2/\sigma^2$, the SE and EE expressions can be simplified into $f_{\text{SE}}(P) = \log_2(1 + \zeta P)$ and $f_{\text{EE}}(P) = \frac{\log_2(1 + \zeta P)}{P + P_f + \chi \log_2(1 + \zeta P)}$. Similarly, by taking the logarithm of the objective function (7a), the subproblem with respect to the transmit power P is given by

$$(\mathbf{P1-5}) : \max_P \beta \ln f_{\text{SE}}(P) + (1 - \beta) \ln f_{\text{EE}}(P) \text{ s.t. } 0 \leq P \leq P_T. \quad (24)$$

To determine the optimal transmit power, it is essential to analyze the properties of $f_{\text{SE}}(P)$ and $f_{\text{EE}}(P)$. Thus, we present the following lemma and proposition.

Lemma 2. There exists one and only one point $P^* \in [0, +\infty)$ that maximizes $f_{\text{EE}}(P)$, and $f_{\text{EE}}(P)$ is strictly increasing and concave at $[0, P^*]$ while strictly decreasing and only quasi-concave at $(P^*, +\infty)$.

Proof: Please refer to Appendix A. ■

Proposition 1. The Pareto optimal set of problem (P1-5) is:

$$\mathcal{P} = \begin{cases} \{P | P = P_T\} & \text{if } P^* \geq P_T, \\ \{P | P^* \leq P \leq P_T\} & \text{if } P^* < P_T. \end{cases} \quad (25)$$

Proof: Please refer to Appendix B. ■

From **Proposition 1**, in the case of $P^* \geq P_T$, the Pareto optimal set \mathcal{P} contains a single point, i.e., P_T , which means that the globally optimal solution for problem (P1-5) is unique.

Therefore, we will then focus on the case when $P^* < P_T$. Let $f_2(P)$ denote the objective function in problem (P1-5), we have

$$f_2(P) = \ln f_{\text{SE}}(P) - (1 - \beta) \ln(P + P_f + \chi f_{\text{SE}}(P)). \quad (26)$$

To maximize $f_2(P)$, we derive its first derivative, which is given by (27) at the bottom of this page. Let $g_2(P)$ denotes the first term in the numerator of (27), i.e.,

$$g_2(P) = \frac{\zeta (P + P_f + \frac{\chi}{\ln 2} \ln(1 + \zeta P))}{(1 + \zeta P + \frac{\chi \zeta}{\ln 2}) \ln(1 + \zeta P)}. \quad (30)$$

Thus, the numerator of $f'_2(P)$ can be expressed as $g_2(P) - (1 - \beta)$. To analyze the roots of the equation $f'_2(P) = 0$, we first need to analyze the monotonicity of function $g_2(P)$, which leads to the following lemma.

Lemma 3. $g_2(P)$ is strictly decreasing with P .

Proof: Please refer to Appendix C. \blacksquare

Setting $f'_2(P) = 0$ yields $g_2(P) = 1 - \beta$. As we previously demonstrated in Lemma 3, $g_2(P)$ is strictly decreasing with P , leading to $0 < g_2(P_T) \leq g_2(P) \leq g_2(P^*)$. Furthermore, recall that P^* is the maximum point of $f_{\text{EE}}(P)$, that is, P^* satisfies $\zeta(P^* + P_f) = (1 + \zeta P^*) \ln(1 + \zeta P^*)$ based on (69). Therefore, we will have

$$\begin{aligned} g_2(P^*) &= \frac{\zeta (P^* + P_f + \frac{\chi}{\ln 2} \ln(1 + \zeta P^*))}{(1 + \zeta P^* + \frac{\chi \zeta}{\ln 2}) \ln(1 + \zeta P^*)} \\ &= \frac{\zeta (P^* + P_f) + \frac{\chi \zeta}{\ln 2} \ln(1 + \zeta P^*)}{\zeta (P^* + P_f) + \frac{\chi \zeta}{\ln 2} \ln(1 + \zeta P^*)} = 1. \end{aligned} \quad (31)$$

From (31) we can know that $g_2(P) \in (0, 1]$, since $1 - \beta \in [0, 1]$, thus, we need to consider the following two cases:

- **Case 1** ($g_2(P_T) > 1 - \beta$): In this case, it is evident that $f'_2(P) > 0$, which means that $f_2(P)$ is strictly increasing with P . Therefore, the optimal transmit power is P_T .
- **Case 2** ($g_2(P_T) \leq 1 - \beta$): In this case, we can know that the equation $g_2(P) = 1 - \beta$ has a unique solution, which is denoted as P^{**} . Therefore, we can infer that when $P \in [P^*, P^{**}]$, $f'_2(P) \geq 0$, which means that $f_2(P)$ is increasing in this interval. When $P \in (P^{**}, P_T]$, $f'_2(P) < 0$, indicating that $f_2(P)$ is decreasing in this interval. The optimal transmit power is P^{**} in this case.

Therefore, the optimal solution for problem (P1-5) is:

$$P_{\text{opt}} = \begin{cases} P_T, & \text{if } P_T \leq P^* \\ P_T, & \text{if } P_T > P^* \text{ and } g_2(P_T) > 1 - \beta \\ P^{**}, & \text{if } P_T > P^* \text{ and } g_2(P_T) \leq 1 - \beta \end{cases} \quad (32)$$

$$f'_2(P) = \frac{\zeta}{\ln(1 + \zeta P)} - (1 - \beta) \frac{1 + \frac{\chi}{\ln 2} \frac{\zeta}{1 + \zeta P}}{P + P_f + \frac{\chi}{\ln 2} \ln(1 + \zeta P)} = \frac{\frac{\zeta (P + P_f + \frac{\chi}{\ln 2} \ln(1 + \zeta P))}{(1 + \zeta P + \frac{\chi \zeta}{\ln 2}) \ln(1 + \zeta P)} - (1 - \beta)}{(1 + \zeta P) \ln(1 + \zeta P) (P + P_f + \frac{\chi}{\ln 2} \ln(1 + \zeta P))} \quad (27)$$

$$g_2(P) = \frac{\zeta P}{(1 + \zeta P + \frac{\chi \zeta}{\ln 2}) \ln(1 + \zeta P)} + \frac{\zeta P_f}{(1 + \zeta P + \frac{\chi \zeta}{\ln 2}) \ln(1 + \zeta P)} + \frac{\frac{\zeta \chi}{\ln 2}}{1 + \zeta P + \frac{\chi \zeta}{\ln 2}} \quad (28)$$

$$\left[\frac{\zeta P}{(1 + \zeta P + A) \ln(1 + \zeta P)} \right]' = \frac{\zeta \ln(1 + \zeta P) + A \zeta \ln(1 + \zeta P) - \zeta^2 P - \frac{\zeta^2 A P}{1 + \zeta P}}{[(1 + \zeta P + A) \ln(1 + \zeta P)]^2} \quad (29)$$

Algorithm 3 Two-Stage joint beamforming design

- 1: **Initialize:** The user location ψ^u .
- 2: Obtain the rough positions of PA based on eq.(14)
- 3: Obtain the optimal positions of PA using **Algorithm 2**.
- 4: Obtain the optimal transmit power based on eq. (32)

Remark 1. Following eq. (32), the optimal transmit power P_{opt} is controlled by 1) the transmit power limit P_T at the BS; 2) the SE-EE weighting factor β ; and 3) the PA positions \mathbf{X} . When $P_T \leq P^*$, both SE and EE increase monotonically with transmit power for all $\beta \in [0, 1]$. Conversely, when $P_T > P^*$, SE and EE become conflicting objectives. These findings necessitates studying the SE-EE trade-off in the regime where $P_T > P^*$, wherein the optimal transmit power achieving the best trade-off is related with β and the configuration of PASS.

E. Overall Algorithm and Convergence

As analyzed in subsection II-C, the optimal \mathbf{X} in (P1-1) is independent of P , whereas the optimal transmit power P depends on \mathbf{X} (see eq. (32)). Consequently, we can first optimize \mathbf{X} under an arbitrarily given P , and then derive the optimal transmit power based on this optimized \mathbf{X} . The exact processes are summarized in **Algorithm 3**. Additionally, **Algorithm 3** is guaranteed to convergence according to **Theorem 1**.

III. JOINT SE-EE DESIGN FOR MULTI-USER PASS

A. System Model

In addition to single-user scenario, the potential of PASS can be further exploited by serving multiple users simultaneously [34], as illustrated in Fig. 2. Thus, let $\mathcal{K} = \{1, 2, \dots, K\}$ denote the set of K single-antenna users, and the position of each user $k \in \mathcal{K}$ is specified as $\psi_k^u = [x_k^u, y_k^u, 0]^T$. Let $\mathbf{s} = [s_1, s_2, \dots, s_K]^T \in \mathbb{C}^{K \times 1}$ denote the vector of transmit signals, where $s_k \in \mathbb{C}$ is the encoded signal for user k . The signals for K users are multiplexed at the baseband using digital transmit beamforming matrix $\mathbf{W} = [\mathbf{w}_1, \mathbf{w}_2, \dots, \mathbf{w}_K] \in \mathbb{C}^{M \times K}$, where \mathbf{w}_k denotes the transmit beamforming vector for user k .

Similar to the single-user scenario, the free-space channel vector between the m -th waveguide and the k -th user can be written as

$$\mathbf{h}_{m,k}^H(\mathbf{x}_m) = \left[\frac{\sqrt{\eta} e^{-j \frac{2\pi}{\lambda} \|\psi_k^u - \boldsymbol{\alpha}_{m,1}\|}}{\|\psi_k^u - \boldsymbol{\alpha}_{m,1}\|}, \dots, \frac{\sqrt{\eta} e^{-j \frac{2\pi}{\lambda} \|\psi_k^u - \boldsymbol{\alpha}_{m,N}\|}}{\|\psi_k^u - \boldsymbol{\alpha}_{m,N}\|} \right], \quad (33)$$

and the overall free-space channel vector $\mathbf{h}_k^H(\mathbf{X}) \in \mathbb{C}^{1 \times MN}$ to user k can be written as

$$\mathbf{h}_k^H(\mathbf{X}) = \left[\mathbf{h}_{1,k}^H(\mathbf{x}_1), \mathbf{h}_{2,k}^H(\mathbf{x}_2), \dots, \mathbf{h}_{M,k}^H(\mathbf{x}_M) \right]. \quad (34)$$

The received signal at user k is given by

$$y_k = \mathbf{h}_k^H(\mathbf{X})\mathbf{G}(\mathbf{X})\mathbf{w}_k s_k + \sum_{i=1, i \neq k}^K \mathbf{h}_k^H(\mathbf{X})\mathbf{G}(\mathbf{X})\mathbf{w}_i s_i + n_k, \quad (35)$$

where $n_k \sim \mathcal{CN}(0, \sigma_k^2)$ is the AWGN at user k with a power of σ_k^2 . The signal-to-interference-plus-noise ratio (SINR) for user k to decode its own signal s_k is given by

$$\gamma_k(\mathbf{W}, \mathbf{X}) = \frac{|\mathbf{h}_k^H(\mathbf{X})\mathbf{G}(\mathbf{X})\mathbf{w}_k|^2}{\sum_{i=1, i \neq k}^K |\mathbf{h}_k^H(\mathbf{X})\mathbf{G}(\mathbf{X})\mathbf{w}_i|^2 + \sigma_k^2}. \quad (36)$$

Consequently, the SE f_{SE} and EE f_{EE} in the PASS-enabled K -user scenario can be expressed as

$$\begin{cases} f_{\text{SE}}(\mathbf{W}, \mathbf{X}) = \sum_{k=1}^K \log_2(1 + \gamma_k(\mathbf{W}, \mathbf{X})), \\ f_{\text{EE}}(\mathbf{W}, \mathbf{X}) = \frac{\sum_{k=1}^K \log_2(1 + \gamma_k(\mathbf{W}, \mathbf{X}))}{\sum_{k=1}^K \|\mathbf{w}_k\|^2 + P_f + \chi f_{\text{SE}}(\mathbf{W}, \mathbf{X})}, \end{cases} \quad (37)$$

where $\sum_{k=1}^K \|\mathbf{w}_k\|^2$ is the overall transmit power.

B. Problem Formulation

Based on (37), the joint SE-EE maximization problem in K -user scenario can be formulated as

$$(\mathbf{P2-1}) : \max_{\mathbf{W}, \mathbf{X}} [f_{\text{SE}}(\mathbf{W}, \mathbf{X})]^\beta \times [f_{\text{EE}}(\mathbf{W}, \mathbf{X})]^{1-\beta} \quad (38a)$$

$$\text{s.t. } (7b), (7c), \quad (38b)$$

$$\sum_{k=1}^K \|\mathbf{w}_k\|^2 \leq P_T, \quad (38c)$$

$$\gamma_k(\mathbf{W}, \mathbf{X}) \geq \gamma_{\text{th}}^k, \forall k, \quad (38d)$$

where the constraint (38c) refers to the constraint on transmit power at the BS side, and γ_{th}^k in (38d) represents the minimum SINR requirement of user k . In this work, the ZF beamforming strategy is adopted. To this end, we first rewritten the signal model in (35) into the following more compact form:

$$\mathbf{y} = \mathbf{H}^H(\mathbf{X})\mathbf{G}(\mathbf{X})\mathbf{W}\mathbf{s} + \mathbf{n} = (\mathbf{G}^H(\mathbf{X})\mathbf{H}(\mathbf{X}))^H\mathbf{W}\mathbf{s} + \mathbf{n}, \quad (39)$$

where $\mathbf{H}(\mathbf{X}) = [\mathbf{h}_1(\mathbf{X}), \mathbf{h}_2(\mathbf{X}), \dots, \mathbf{h}_K(\mathbf{X})] \in \mathbb{C}^{MN \times K}$ is the overall channel matrix, and $\mathbf{n} \in \mathbb{C}^{K \times 1}$ represents the noise vector. Let $\Psi(\mathbf{X}) \triangleq \mathbf{G}^H(\mathbf{X})\mathbf{H}(\mathbf{X}) \in \mathbb{C}^{M \times K}$, given that $M \geq K$, we can obtain the following ZF beamforming matrix for arbitrary \mathbf{X} :

$$\mathbf{W} = \Psi(\mathbf{X})(\Psi^H(\mathbf{X})\Psi(\mathbf{X}))^{-1}\mathbf{P}^{\frac{1}{2}}, \quad (40)$$

where $\mathbf{P} = \text{diag}\{P_1, P_2, \dots, P_K\} \in \mathbb{C}^{K \times K}$ is the diagonal power control matrix, and P_k is the power coefficient for user k . Therefore, the transmit power can be reformulated as

$$\begin{aligned} \sum_{k=1}^K \|\mathbf{w}_k\|^2 &= \text{tr}(\mathbf{W}\mathbf{W}^H) \\ &= \text{tr}(\Psi(\mathbf{X})(\Psi^H(\mathbf{X})\Psi(\mathbf{X}))^{-1}\mathbf{P}(\Psi^H(\mathbf{X})\Psi(\mathbf{X}))^{-1}\Psi^H(\mathbf{X})) \\ &= \text{tr}((\Psi^H(\mathbf{X})\Psi(\mathbf{X}))^{-1}\Psi^H(\mathbf{X})\Psi(\mathbf{X})(\Psi^H(\mathbf{X})\Psi(\mathbf{X}))^{-1}\mathbf{P}) \\ &= \text{tr}((\Psi^H(\mathbf{X})\Psi(\mathbf{X}))^{-1}\mathbf{P}). \end{aligned} \quad (41)$$

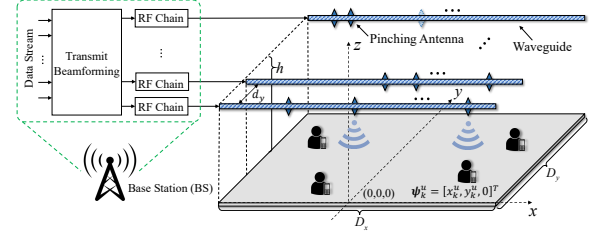


Fig. 2. System model for PASS-enabled multi-user communications.

Substituting (41) into (36) yields $\gamma_k = P_k/\sigma_k^2$. Then, problem (P2-1) becomes

$$(\mathbf{P2-2}) : \max_{\mathbf{P}, \mathbf{X}} \beta \ln(f_{\text{SE}}(\mathbf{P}, \mathbf{X})) + (1-\beta) \ln(f_{\text{EE}}(\mathbf{P}, \mathbf{X})) \quad (42a)$$

$$\text{s.t. } (7b), (7c), \quad (42b)$$

$$\text{tr}((\Psi^H(\mathbf{X})\Psi(\mathbf{X}))^{-1}\mathbf{P}) \leq P_T, \quad (42c)$$

$$P_k/\sigma_k^2 \geq \gamma_{\text{th}}^k. \quad (42d)$$

It is observed that the power control matrix \mathbf{P} is still coupled with the PA positions \mathbf{X} through (42c). In the following, we first divide the problem (P2-2) into two subproblems: pinching beamforming optimization with fixed power control matrix, and power optimization with fixed PA positions. Thus, an alternating iterative algorithm of these two sub-problems is presented to get the sub-optimal solutions for problem (P2-2).

C. Optimization of PA Positions

When given the power control matrix \mathbf{P} , the sub-problem for optimizing pinching beamforming can be written as

$$(\mathbf{P2-3}) : \min_{\mathbf{X}} \text{tr}((\Psi^H(\mathbf{X})\Psi(\mathbf{X}))^{-1}\mathbf{P}) \quad (43a)$$

$$\text{s.t. } (7b), (7c), (42c). \quad (43b)$$

The objective function in (P2-3) takes the form of (43a) because, for a given \mathbf{P} , expanding (42a) reveals that it depends solely on the term $\text{tr}((\Psi^H(\mathbf{X})\Psi(\mathbf{X}))^{-1}\mathbf{P})$. Therefore, minimizing $\text{tr}((\Psi^H(\mathbf{X})\Psi(\mathbf{X}))^{-1}\mathbf{P})$ is equivalent to maximizing the original objective function (42a).

For the inequality constraint (42c), we can integrate it into the objective function using the penalty method. Hence, problem (P2-3) can be reformulated as

$$\begin{aligned} (\mathbf{P2-4}) : \min_{\mathbf{X}} & \text{tr}((\Psi^H(\mathbf{X})\Psi(\mathbf{X}))^{-1}\mathbf{P}) \\ & + \tau \left(\left[\text{tr}((\Psi^H(\mathbf{X})\Psi(\mathbf{X}))^{-1}\mathbf{P}) - P_T \right]^+ \right)^2 \end{aligned} \quad (44a)$$

$$\text{s.t. } (7b), (7c), \quad (44b)$$

where $[x]^+$ is defined as $\max(0, x)$, and τ is the penalty coefficient corresponding to the constraint (42c). The problem can be solved via an element-wise one-dimensional search where in one iteration, the x -axis coordinate of each PA $x_{m,n}^p$ is optimized sequentially over a certain range, by keeping all other PAs fixed. However, we notice that when optimizing

$x_{m,n}^p$, the matrix inversion $(\Psi^H(\mathbf{X})\Psi(\mathbf{X}))^{-1}$ must be computed at each candidate solution, which results in significant computational complexity. To address this, we first present a matrix decomposition method. Recall that $\Psi^H(\mathbf{X}) \in \mathbb{C}^{K \times M}$ can be expressed as

$$\Psi^H(\mathbf{X}) = \begin{bmatrix} \mathbf{h}_{1,1}^H(\mathbf{x}_1)\mathbf{g}_1(\mathbf{x}_1) & \cdots & \mathbf{h}_{M,1}^H(\mathbf{x}_M)\mathbf{g}_M(\mathbf{x}_M) \\ \mathbf{h}_{1,2}^H(\mathbf{x}_1)\mathbf{g}_1(\mathbf{x}_1) & \cdots & \mathbf{h}_{M,2}^H(\mathbf{x}_M)\mathbf{g}_M(\mathbf{x}_M) \\ \vdots & \ddots & \vdots \\ \mathbf{h}_{1,K}^H(\mathbf{x}_1)\mathbf{g}_1(\mathbf{x}_1) & \cdots & \mathbf{h}_{M,K}^H(\mathbf{x}_M)\mathbf{g}_M(\mathbf{x}_M) \end{bmatrix}, \quad (45)$$

where the k -th element in the m -th column of $\Psi^H(\mathbf{X})$ represents the aggregate channel coefficient from all PAs on the m -th waveguide to the user k . Denote $\mathbf{a}_m \in \mathbb{C}^{K \times 1}$ as the m -th column vector of $\Psi^H(\mathbf{X})$. Then, $\Psi^H(\mathbf{X})$ can be rewritten as $\Psi^H(\mathbf{X}) = [\mathbf{a}_1, \mathbf{a}_2, \dots, \mathbf{a}_M]$, leading to the following transformation:

$$\Psi^H(\mathbf{X})\Psi(\mathbf{X}) = \sum_{m=1}^M \mathbf{a}_m \mathbf{a}_m^H, \quad (46)$$

where $\mathbf{a}_m \mathbf{a}_m^H \in \mathbb{C}^{K \times K}$. For optimizing the PA positions on the m -th waveguide, (46) can be written as

$$\Psi^H(\mathbf{X})\Psi(\mathbf{X}) = \mathbf{a}_m \mathbf{a}_m^H + \sum_{m'=1, m' \neq m}^M \mathbf{a}_{m'} \mathbf{a}_{m'}^H. \quad (47)$$

Let $\mathbf{B}_m \triangleq \sum_{m'=1, m' \neq m}^M \mathbf{a}_{m'} \mathbf{a}_{m'}^H$. Given that $M \geq K$, the matrix \mathbf{B}_m must be full-rank. Therefore, by using Sherman-Morrison formula, we have

$$\begin{aligned} (\Psi^H(\mathbf{X})\Psi(\mathbf{X}))^{-1} &= (\mathbf{a}_m \mathbf{a}_m^H + \mathbf{B}_m)^{-1} \\ &= (\mathbf{B}_m)^{-1} - \frac{(\mathbf{B}_m)^{-1} \mathbf{a}_m \mathbf{a}_m^H (\mathbf{B}_m)^{-1}}{1 + \mathbf{a}_m^H (\mathbf{B}_m)^{-1} \mathbf{a}_m}. \end{aligned} \quad (48)$$

Consequently, by substituting eq. (48) into eq. (43a), the objective function of problem (P2-3) can be expressed as

$$\begin{aligned} \text{tr}((\Psi^H(\mathbf{X})\Psi(\mathbf{X}))^{-1} \mathbf{P}) &= \text{tr}((\mathbf{B}_m)^{-1} \mathbf{P}) - \text{tr}\left(\frac{(\mathbf{B}_m)^{-1} \mathbf{a}_m \mathbf{a}_m^H (\mathbf{B}_m)^{-1} \mathbf{P}}{1 + \mathbf{a}_m^H (\mathbf{B}_m)^{-1} \mathbf{a}_m}\right) \\ &= \text{tr}((\mathbf{B}_m)^{-1} \mathbf{P}) - \frac{\text{tr}(\mathbf{a}_m^H (\mathbf{B}_m)^{-1} \mathbf{P} (\mathbf{B}_m)^{-1} \mathbf{a}_m)}{1 + \mathbf{a}_m^H (\mathbf{B}_m)^{-1} \mathbf{a}_m} \\ &= \text{tr}((\mathbf{B}_m)^{-1} \mathbf{P}) - \frac{\mathbf{a}_m^H (\mathbf{B}_m)^{-1} \mathbf{P} (\mathbf{B}_m)^{-1} \mathbf{a}_m}{1 + \mathbf{a}_m^H (\mathbf{B}_m)^{-1} \mathbf{a}_m}. \end{aligned} \quad (49)$$

Based on (49), the optimization problem for $x_{m,n}^p$ can be formulated as

$$(\mathbf{P2-5}) : \min_{x_{m,n}^p} f_{\text{obj}}(x_{m,n}^p) \quad (50a)$$

$$\text{s.t. } x_{m,n}^p \in \mathcal{S}_{m,n}, \quad (50b)$$

where $f_{\text{obj}}(x_{m,n}^p)$ is expressed as

$$\begin{aligned} f_{\text{obj}}(x_{m,n}^p) &= \text{tr}((\mathbf{B}_m)^{-1} \mathbf{P}) - \frac{\mathbf{a}_m^H (\mathbf{B}_m)^{-1} \mathbf{P} (\mathbf{B}_m)^{-1} \mathbf{a}_m}{1 + \mathbf{a}_m^H (\mathbf{B}_m)^{-1} \mathbf{a}_m} \\ &+ \tau \left(\left[\text{tr}((\mathbf{B}_m)^{-1} \mathbf{P}) - \frac{\mathbf{a}_m^H (\mathbf{B}_m)^{-1} \mathbf{P} (\mathbf{B}_m)^{-1} \mathbf{a}_m}{1 + \mathbf{a}_m^H (\mathbf{B}_m)^{-1} \mathbf{a}_m} - P_T \right]^+ \right]^2. \end{aligned} \quad (51)$$

$\mathcal{S}_{m,n}$ in constraint (50b) is defined as the feasible range of $x_{m,n}^p$, which can be expressed as

$$\mathcal{S}_{m,n} = [x_{m,n-1}^p + \Delta_{\min}, x_{m,n+1}^p - \Delta_{\min}] \cap [0, D_x]. \quad (52)$$

The decomposition method in (47) allows the inverse of matrix to be computed just once for all candidate solutions of $x_{m,n}^p$, significantly reduce the computational complexity. For problem (P2-5), we employ particle swarm optimization (PSO) algorithm. The PSO operates with L particles, each characterized by its “position” and “velocity”. The “position” of each particle represents a candidate solution for (P2-5). For brevity, the full procedure of PSO will not be restated in this paper, instead, the pinching beamforming optimization algorithm is summarized in **Algorithm 4**.

D. Optimization of Transmit Power

To facilitate the optimization of power control matrix \mathbf{P} , the original problem (P2-2) can be transformed into the following equivalent form for a given \mathbf{X} :

$$(\mathbf{P2-6}) : \max_{\mathbf{P}} \beta \ln(f_{\text{SE}}(\mathbf{P})) + (1-\beta) \ln(f_{\text{EE}}(\mathbf{P})) \quad (53a)$$

$$\text{s.t. } \text{tr}(\mathbf{A}\mathbf{P}) \leq P_T, \quad (53b)$$

$$P_k / \sigma_k^2 \geq \gamma_k^{\text{th}}, \quad (53c)$$

where $\Lambda \triangleq (\Psi^H(\mathbf{X})\Psi(\mathbf{X}))^{-1}$. It is evident that all constraints are convex, so we only need to tackle the non-convexity of the objective function (53a). First, we introduce two slack variables μ_1 and μ_2 such that

$$\beta \ln(f_{\text{SE}}(\mathbf{P})) \geq \mu_1, \quad (54)$$

$$(1-\beta) \ln(f_{\text{EE}}(\mathbf{P})) \geq \mu_2. \quad (55)$$

With the help of these two slack variables, problem (P2-6) can be equivalently written as

$$(\mathbf{P2-7}) : \max_{\mathbf{P}, \mu_1, \mu_2} \mu_1 + \mu_2 \quad (56a)$$

$$\text{s.t. } (53b), (53c), (54), (55). \quad (56b)$$

It can be observed that now (56a) is a linear function in terms of μ_1 and μ_2 . For constraint (54), it can be rewritten as

$$e^{\frac{\mu_1}{\beta}} - \sum_{k=1}^K \log_2 \left(1 + \frac{P_k}{\sigma_k^2} \right) \leq 0. \quad (57)$$

It is evident that (57) is convex when $\beta > 0$.³ For (55), we have

$$\frac{\sum_{k=1}^K \log_2 \left(1 + \frac{P_k}{\sigma_k^2} \right)}{\text{tr}(\mathbf{A}\mathbf{P}) + P_f + \chi \sum_{k=1}^K \log_2 \left(1 + \frac{P_k}{\sigma_k^2} \right)} \geq e^{\frac{\mu_2}{1-\beta}}. \quad (58)$$

To handle the non-convexity of (58), we introduce a new slack variable κ such that

$$\frac{\sum_{k=1}^K \log_2 \left(1 + \frac{P_k}{\sigma_k^2} \right)}{\text{tr}(\mathbf{A}\mathbf{P}) + P_f + \chi \sum_{k=1}^K \log_2 \left(1 + \frac{P_k}{\sigma_k^2} \right)} \geq \frac{e^{\frac{\mu_2}{1-\beta}} \kappa}{\kappa}. \quad (59)$$

Therefore, the original constraint (55) can be split into the following two constraints:

$$\sum_{k=1}^K \log_2 \left(1 + \frac{P_k}{\sigma_k^2} \right) \geq e^{\frac{\mu_2}{1-\beta}} \kappa, \quad (60)$$

³It should be noted that when $\beta = 0$, (P2-6) reduces to the EE maximization problem, and hence, constraint (54) ceases to exist.

$$\text{tr}(\mathbf{AP}) + P_f + \chi \sum_{k=1}^K \log_2 \left(1 + \frac{P_k}{\sigma_k^2} \right) \leq \kappa. \quad (61)$$

For (60), the variables μ_2 and κ are coupled, but we notice that $u(\mu_2, \kappa) = e^{\frac{\mu_2}{1-\beta}} \kappa$ is a twice-differentiable function when $\beta \neq 1^4$, its second-order Taylor expansion around a given point $(\mu_2^{(l)}, \kappa^{(l)})$ can be expressed as

$$u(\mu_2, \kappa) \approx e^{\frac{\mu_2^{(l)}}{1-\beta}} \kappa^{(l)} + \frac{1}{1-\beta} e^{\frac{\mu_2^{(l)}}{1-\beta}} \kappa^{(l)} (\mu_2 - \mu_2^{(l)}) + e^{\frac{\mu_2^{(l)}}{1-\beta}} (\kappa - \kappa^{(l)}) + \frac{1}{2} \left[\left[\mu_2 - \mu_2^{(l)}, \kappa - \kappa^{(l)} \right] \nabla^2 u(\mu_2^{(l)}, \kappa^{(l)}) \left[\mu_2 - \mu_2^{(l)}, \kappa - \kappa^{(l)} \right]^T \right], \quad (62)$$

where l is the iteration index of successive convex approximation (SCA). However, if we simply substitute eq. (62) into constraint (60), the obtained solution may not satisfy the constraints of the original problem. According to the lemma 1 in [35], by upper-bounding the Hessian matrix via $\nabla^2 u(\mu_2^{(l)}, \kappa^{(l)}) \preceq \delta \mathbf{I}$, where $\delta \in \mathbb{R}_+$, we can get the convex upper bound of $u(\mu_2, \kappa)$ around point $(\mu_2^{(l)}, \kappa^{(l)})$ as

$$u(\mu_2, \kappa) \leq e^{\frac{\mu_2^{(l)}}{1-\beta}} \kappa^{(l)} + \frac{1}{1-\beta} e^{\frac{\mu_2^{(l)}}{1-\beta}} \kappa^{(l)} (\mu_2 - \mu_2^{(l)}) + e^{\frac{\mu_2^{(l)}}{1-\beta}} (\kappa - \kappa^{(l)}) + \frac{\delta}{2} \left[(\mu_2 - \mu_2^{(l)})^2 + (\kappa - \kappa^{(l)})^2 \right] = U^{(l)}(\mu_2, \kappa). \quad (63)$$

In (63), we set δ as the maximum eigenvalue of the Hessian matrix $\nabla^2 u(\mu_2^{(l)}, \kappa^{(l)})$. Consequently, the original constraint (60) now becomes $U^{(l)}(\mu_2, \kappa) - \sum_{k=1}^K \log_2 (1 + P_k / \sigma_k^2) \leq 0$, which is convex.

For constraint (61), the function $\log_2(1 + P_k / \sigma_k^2)$ is concave with respect to P_k . Since any concave function is globally upper-bounded by its first-order Taylor expansion at any point, we can derive an upper bound for $\log_2(1 + P_k / \sigma_k^2)$ at the given local point $P_k^{(l)}$ in the l -th iteration as

$$\log_2(1 + \frac{P_k}{\sigma_k^2}) \leq \log_2(1 + \frac{P_k^{(l)}}{\sigma_k^2}) + \frac{P_k - P_k^{(l)}}{(\ln 2)(\sigma_k^2 + P_k^{(l)})} = g_k^{(l)}(P_k), \quad (64)$$

thus, we can convert (61) into the following convex constraint:

$$\text{tr}(\mathbf{AP}) + P_f + \chi \sum_{k=1}^K g_k^{(l)}(P_k) - \kappa \leq 0. \quad (65)$$

Based on the above approximations, the problem (P2-7) can be further reformulated as

$$(\mathbf{P2-8}) : \max_{\Xi} \mu_1 + \mu_2 \quad (66a)$$

$$\text{s.t. } (53b), (53c), (57), \quad (66b)$$

$$U^{(l)}(\mu_2, \kappa) - \sum_{k=1}^K \log_2 \left(1 + \frac{P_k}{\sigma_k^2} \right) \leq 0, \quad (66c)$$

$$\text{tr}(\mathbf{AP}) + P_f + \chi \sum_{k=1}^K g_k^{(l)}(P_k) - \kappa \leq 0, \quad (66d)$$

where $\Xi = \{\mathbf{P}, \mu_1, \mu_2, \kappa\}$ consists of all the variables involved in this design. Now, problem (P2-8) is convex and therefore

⁴When $\beta = 1$, (P2-6) reduces to the SE maximization problem, and constraint (55) ceases to exist.

Algorithm 4 Proposed Method for Solving (P2-4)

- 1: **Initialize:** Set iteration index $r=1$, initial variables $\mathbf{X}^{(r)}$, power control matrix \mathbf{P} , and convergence tolerance $0 \leq \epsilon_1 \ll 0$.
- 2: **repeat**
- 3: **for** $m \in \{1, 2, \dots, M\}$ **do**
- 4: **for** $n \in \{1, 2, \dots, N\}$ **do**
- 5: Update $x_{m,n}^p$ by solving problem (P2-5) through PSO for given \mathbf{P}
- 6: **end for**
- 7: **end for**
- 8: Set $r = r + 1$
- 9: **until** The fractional decrease of the objective value of problem (P2-4) is below a threshold ϵ_1

Algorithm 5 ZF-based BCD Algorithm for Solving (P2-2)

- 1: **Initialize:** Set iteration index $q=1$, initial variables $\mathbf{X}^{(q)}$, $\mu_2^{(q)}$, $\kappa^{(q)}$, $\mathbf{P}^{(q)}$, and convergence tolerance $0 \leq \epsilon_2 \ll 0$.
- 2: **repeat**
- 3: Set iteration index $l=1$, error tolerance $0 \leq \epsilon_3 \ll 1$
- 4: Set $\mu_2^{(l)} = \mu_2^{(q)}$, $\kappa^{(l)} = \kappa^{(q)}$, and $\mathbf{P}^{(l)} = \mathbf{P}^{(q)}$
- 5: **repeat**
- 6: Solve (P2-8) for given $\mathbf{X}^{(q)}, \mu_2^{(l)}, \kappa^{(l)}$ and $\mathbf{P}^{(l)}$
- 7: Updating $\mu_2^{(l+1)}, \kappa^{(l+1)}$ and $\mathbf{P}^{(l+1)}$
- 8: Set $l = l + 1$
- 9: **until** The fractional increase of the objective value of problem (P2-8) is below a threshold ϵ_3
- 10: Denote the optimal power control matrix as $\mathbf{P}^{(q+1)}$
- 11: Obtain the optimal positions of PASS $\mathbf{X}^{(q+1)}$ by using **Algorithm 4** for given $\mathbf{P}^{(q+1)}$
- 12: Set $q = q + 1$
- 13: **until** The fractional increase of the objective value of problem (P2-2) is below a threshold ϵ_2

can be solved optimally by standard convex program solvers such as CVX.

E. Overall Algorithm and Convergence

Building on the results from previous two subsections, we present an overall iterative algorithm for problem (P2-2) based on block coordinate descent (BCD) method. Specifically, the entire optimization variables in original problem (P2-2) are partitioned into two blocks, i.e., $\{\mathbf{P}, \mathbf{X}\}$. Then, the power control matrix \mathbf{P} and the PA positions \mathbf{X} are alternately optimized, by solving problem (P2-8) and (P2-4) correspondingly, while keeping the other variable fixed. The obtained solution from each iteration is used as the input in the subsequent one. The ZF-based BCD algorithm for problem (P2-2) is summarized in **Algorithm 5**.

Next, we provide the analysis of the convergence of **Algorithm 5**. Since a new slack variable κ is introduced when handling problem (P2-7), we define an intermediate optimization problem (P2-7-1) as

$$(\mathbf{P2-7-1}) : \max_{\mathbf{P}, \mu_1, \mu_2, \kappa} \mu_1 + \mu_2 \quad (67a)$$

$$\text{s.t. } (53b), (53c), (57), (60), (61). \quad (67b)$$

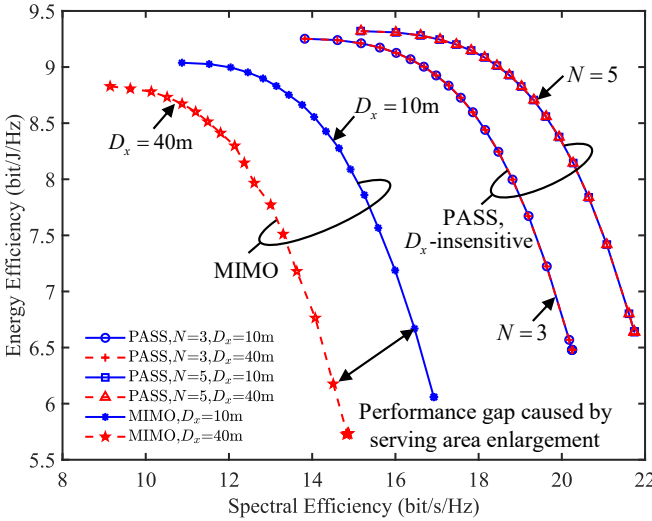


Fig. 3. The SE-EE trade-off in single-user case.

It is noticed that problem **(P2-6)**, **(P2-7)** and **(P2-7-1)** are equivalent. For given $\mathbf{X}^{(q)}$, $\mathbf{P}^{(q)}$, $\mu_1^{(q)}$, $\mu_2^{(q)}$ and $\kappa^{(q)}$ in steps 3-10 of **Algorithm 5**, we have

$$\begin{aligned}
& O_{(\mathbf{P2-2})} \left(\mathbf{X}^{(q)}, \mathbf{P}^{(q)} \right) \stackrel{(a)}{=} O_{(\mathbf{P2-6})} \left(\mathbf{X}^{(q)}, \mathbf{P}^{(q)} \right) \\
& = O_{(\mathbf{P2-7-1})} \left(\mathbf{X}^{(q)}, \mathbf{P}^{(q)}, \mu_1^{(q)}, \mu_2^{(q)}, \kappa^{(q)} \right) \\
& \stackrel{(b)}{=} O_{(\mathbf{P2-8})} \left(\mathbf{X}^{(q)}, \mathbf{P}^{(q)}, \mu_1^{(q)}, \mu_2^{(q)}, \kappa^{(q)} \right) \\
& \stackrel{(c)}{\leq} O_{(\mathbf{P2-8})} \left(\mathbf{X}^{(q)}, \mathbf{P}^{(q+1)}, \mu_1^{(q+1)}, \mu_2^{(q+1)}, \kappa^{(q+1)} \right) \\
& \stackrel{(d)}{\leq} O_{(\mathbf{P2-7-1})} \left(\mathbf{X}^{(q)}, \mathbf{P}^{(q+1)}, \mu_1^{(q+1)}, \mu_2^{(q+1)}, \kappa^{(q+1)} \right) \\
& = O_{(\mathbf{P2-6})} \left(\mathbf{X}^{(q)}, \mathbf{P}^{(q+1)} \right) \stackrel{(e)}{=} O_{(\mathbf{P2-2})} \left(\mathbf{X}^{(q)}, \mathbf{P}^{(q+1)} \right) \\
& \stackrel{(f)}{\leq} O_{(\mathbf{P2-2})} \left(\mathbf{X}^{(q+1)}, \mathbf{P}^{(q+1)} \right), \tag{68}
\end{aligned}$$

where $O_{(\cdot)}$ represents the objective value of different problem. (a) and (e) hold since **(P2-2)** and **(P2-6)** have the same objective function value at any feasible \mathbf{P} with given PA positions \mathbf{X} , (b) holds the Taylor expansions in (63) and (64) are tight at the given local points, (c) holds since in steps 3-10 of **Algorithm 5**, problem **(P2-8)** is solved optimally with solution $\{\mathbf{P}^{(q+1)}, \mu_1^{(q+1)}, \mu_2^{(q+1)}, \kappa^{(q+1)}\}$ under the given $\mathbf{X}^{(q)}$, (d) holds since the objective value of problem **(P2-8)** is the lower bound of that of problem **(P2-7-1)**, and (f) holds since the monotonic convergence is guaranteed in PSO method when the final solution satisfy the constraint (42c). On the other hand, the objective value of problem **(P2-2)** is upper bounded by a finite value. Therefore, the proposed **Algorithm 5** is guaranteed to converge.

IV. NUMERICAL RESULTS

In this section, numerical results are provided to illustrate the effectiveness of our proposed SE-EE tradeoff design of a PASS-assisted downlink system. Without loss of generality, we consider $M=4$ waveguides with a height of $h=3$ m. The

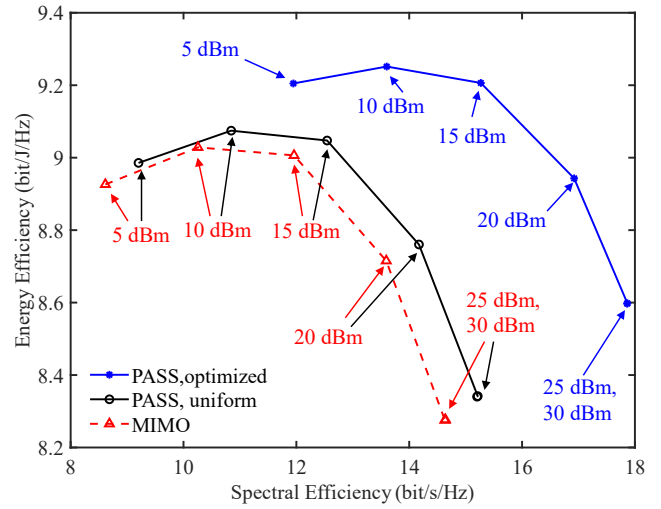


Fig. 4. SE and EE performance in single-user case under different P_T , with $\beta=0.5$.

other simulation parameters are set as follows: $D_y=10$ m, the noise power is -90 dBm, the minimum SINR of all users is set to 6 dB, f_c is 28 GHz, $\Delta_{\min} = \lambda/2$, $n_{\text{neff}} = 1.4$, $P_f=0.1$ Watts, and $\chi=0.1$. For PSO, we employ a swarm of 30 particles over 300 iterations, with inertia weight, penalty coefficient τ , cognitive, and social parameters set to 0.7298, 10^4 , 1.4962 and 1.4962, respectively.

A. Single-User System

Fig. 3 compares the SE-EE tradeoff in PASS and conventional MIMO system in a single-user scenario.⁵ Each point on the curve corresponds to the SE and EE pair of the optimal solutions obtained at a specific β , which takes values from 0 to 1 in steps of 0.05. It is observed that PASS consistently outperforms MIMO in terms of the joint SE-EE performance, and this gain becomes more pronounced as the number of PAs N increases. Furthermore, while the performance of MIMO degrades significantly with a larger D_x , PASS exhibits insensitivity to this parameter. A notable observation is that for $N=5$ and $D_x=40$ m, PASS at $\beta=0$ can even achieve a higher SE than MIMO at $\beta=1$. In Fig. 4, we compare the SE-EE performance under $\beta=0.5$ to highlight the necessity of jointly optimizing the transmit power and the pinching beamforming. The black line represents a baseline of uniformly placed PAs under optimized transmit power. Results show that joint optimization yields better joint SE-EE performance under the same transmit power constraint P_T at the BS. Moreover, we notice that even with uniform PA placement, the joint SE-EE performance of the system are still better than that of the conventional MIMO, which indicates that PASS is beneficial for boosting the SE and EE of the system.

B. Multi-User System

Fig. 5 illustrates the convergence behavior of the proposed algorithms. Specifically, the convergence behavior of

⁵For fairness, the number of RF chains of MIMO and PASS is consistent, and the MIMO BS is positioned at the center of the service region.

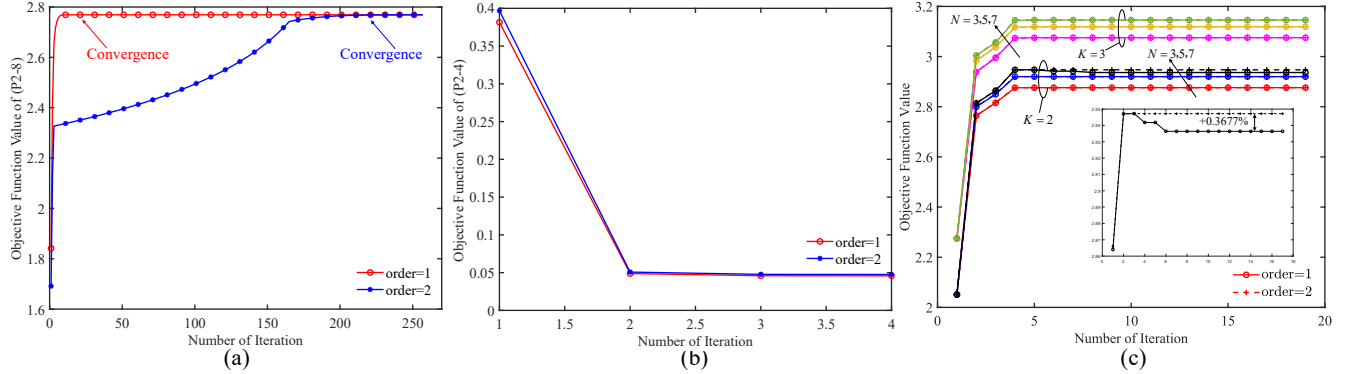


Fig. 5. Convergence of (a) the objective function in (P2-8), (b) the objective function in (P2-4), and (c) the Algorithm 5.

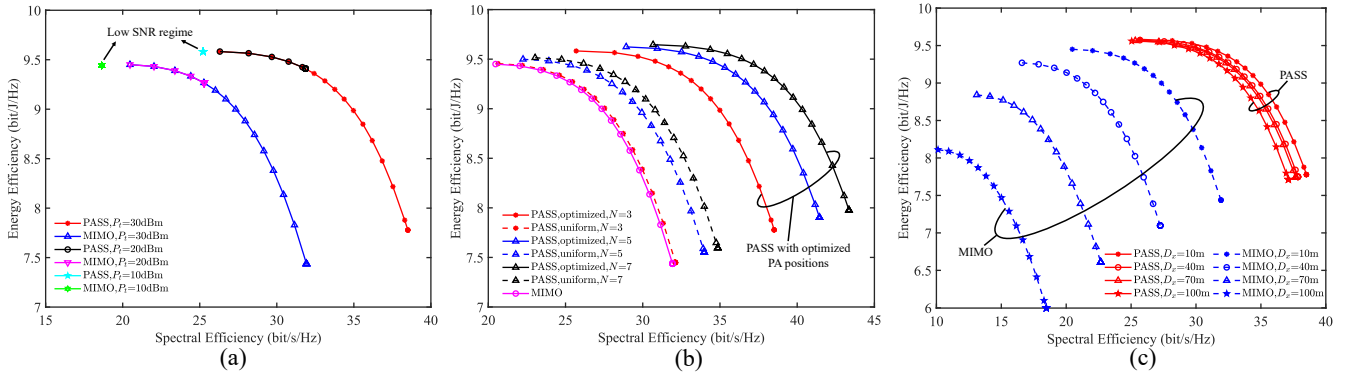


Fig. 6. The SE-EE trade-off under different (a) P_T , (b) N , and (c) D_x .

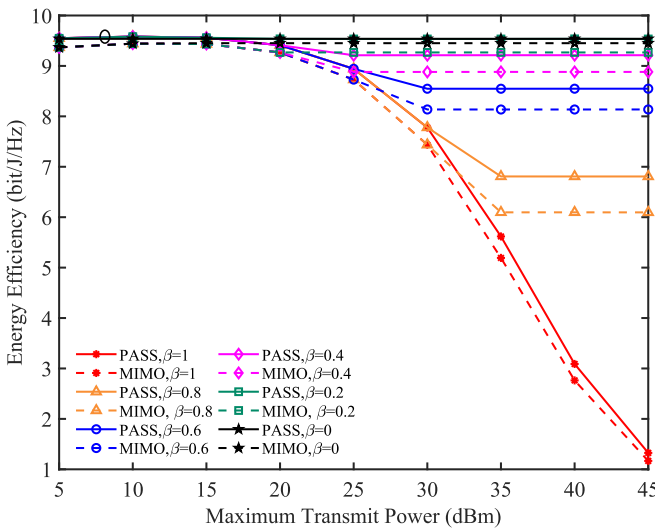


Fig. 7. Achieved EE versus P_T for various β .

the objective function in (P2-8) is shown in Fig. 5(a). The red and blue curves represent different expansion schemes for $u(\mu_2, \kappa)$ in eq. (60), corresponding to the first-order and second-order Taylor expansions, respectively. It can be observed that although the first-order Taylor expansion scheme does not guarantee the monotonic increasing property of the overall objective function (as will be shown in Fig. 5(c)),

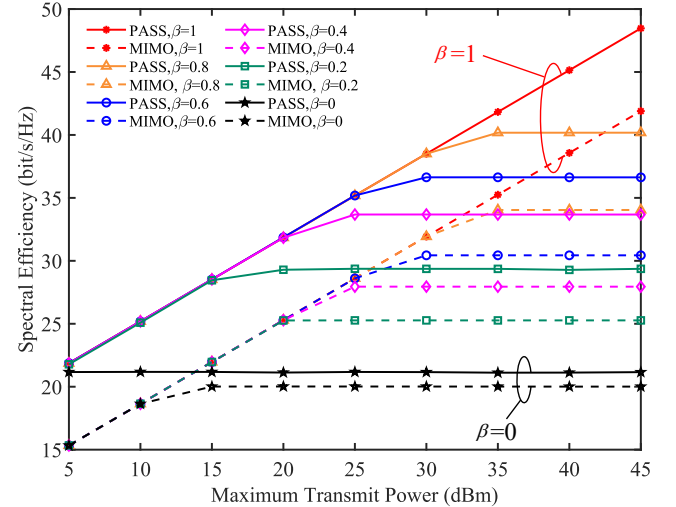


Fig. 8. Achieved SE versus P_T for various β .

it achieves significantly faster convergence speed on (P2-8) compared to the using second-order Taylor expansion, while both approaches converge to the same optimal value. Fig. 5(b) shows the convergence behavior of the objective function in (P2-4), and in Fig. 5(c), the convergence of Algorithm 5 for different N and K is demonstrated. The threshold ϵ_2 to terminate the algorithm has been set to 10^{-6} . As shown in Fig.

5(c), the overall algorithm converges rapidly with both first- and second-order Taylor expansions. However, given the faster convergence rate of the first-order Taylor expansion when solving (P2-8), it is adopted in the subsequent simulations.

Fig. 6(a) shows the SE-EE tradeoff of PASS and conventional MIMO system under different P_T while keeping $D_x=D_y=10$ m, $N=3$, and $K=2$. When $P_T=30$ dBm, a tradeoff between SE and EE exists in both PASS and MIMO. However, this trade-off vanishes when P_T is reduced to 10 dBm, where both SE and EE remain unchanged in the range of β from 0 to 1. This is because the Pareto optimal set for problem (P2-6) degenerates to a single point P_T . Fig. 6(b) illustrates the SE-EE tradeoff under different number of PAs with $P_T=30$ dBm and $K=2$. The dashed line denotes the uniform PA placement strategy. It can be observed that the SE-EE tradeoff regime gap between MIMO and PASS increases as the number of PAs increases. Furthermore, we notice that the joint optimization of power control matrix and pinching beamforming achieves the best performance compared with the baselines. Fig. 6(c) illustrates the effect of D_x on the SE-EE tradeoff with $P_T=30$ dBm, $N=2$, and $K=2$. It can be seen that expanding the service area significantly degrades the performance of MIMO system. In contrast, PASS is considerably less affected by an increase in D_x , due to its capacity to flexibly reposition the PAs to mitigate the large-scale path loss.

Fig. 7 illustrates the achieved EE of the system versus P_T for various weighting coefficients β . Specifically, when $\beta=0$, the original problem becomes a EE-maximization design for both PASS and MIMO system. Take PASS as an example, its EE remains almost unchanged. On the other hand, when $\beta=1$, the original problem turns into a SE-maximization design. Unlike the EE-maximization counterpart, the EE of both PASS and MIMO starts to decline at higher available power levels since SE-maximization design aims to maximize the sum rate at the cost of EE degradation, but it is worth noting that for $\forall \beta \in [0, 1]$, PASS always achieves better EE performance compared with MIMO system, which reflects that PASS is an energy-efficient architecture.

Fig. 8 shows the SE comparison versus P_T for various β . When $\beta=1$, the original SE-EE tradeoff design becomes conventional SE-maximization, in this case, the SE of both PASS and MIMO are increasing linearly with P_T under ZF beamforming strategy. When $\beta=0$, the original problem turns out to be a EE-maximization design in which SE increases with P_T until it reaches the “green power” as described in [32], and then SE and EE saturate. Similarly, it is also observed that under the same setting, PASS always achieves better SE performance compared with MIMO under different P_T and β .

V. CONCLUSION

A joint transmit and pinching beamforming design to address the SE-EE tradeoff in both PASS-enabled single- and multi-user scenarios were investigated. In the single-user scenario, a two-stage joint beamforming design is proposed: In the first stage, ICR was proposed to align the phases of the received signals, and a PA placement framework was proposed based on ICR. In the second stage, the closed-form solution

for the optimal transmit power was derived with the given optimized PA positions under the MRT strategy. In multi-user scenario, a ZF-assisted AO algorithm was proposed to tackle the non-convex joint transmit and pinching beamforming problem. The power allocation subproblem was addressed by deriving the convex upper bounds of the constraints, and the pinching beamforming was optimized through an iterative element-wise sequential PSO method. The numerical results demonstrated that PASS significantly improved SE and EE performance compared to conventional MIMO systems, with the regime gap becoming more pronounced when the number of PAs and service region increased. These findings reveal the great potential of PASS in the next-generation wireless networks, as a spectral- and energy-efficient architecture.

APPENDIX A PROOF OF LEMMA 2

Take the first-order derivative of $f_{\text{EE}}(P)$ as

$$[f_{\text{EE}}(P)]' = \frac{\zeta(P+P_f) - (1+\zeta P)\ln(1+\zeta P)}{(1+\zeta P)(P+P_f + \frac{\chi}{\ln 2}\ln(1+\zeta P))^2 \ln 2}. \quad (69)$$

We notice that the denominator of $[f_{\text{EE}}(P)]'$ is positive. For the numerator, letting $g(P) = \zeta(P+P_f) - (1+\zeta P)\ln(1+\zeta P)$, we have $g'(P) = -\zeta \ln(1+\zeta P) < 0$, implying that $g(P)$ is decreasing with P . Furthermore, $\lim_{P \rightarrow 0^+} g(P) = \zeta P_f > 0$, $\lim_{P \rightarrow +\infty} g(P) = -\infty$. Therefore, the equation $g(P) = 0$ has a unique root on $[0, +\infty)$, denoted as P^* , and $f_{\text{EE}}(P)$ is monotonically increasing on $[0, P^*)$, and monotonically decreasing on $(P^*, +\infty)$. Meanwhile, letting $l(p)$ represent the denominator part of (69), we can obtain the second-order derivative of $f_{\text{EE}}(P)$ with P as

$$[f_{\text{EE}}(P)]'' = \frac{g'(P)l(P) - g(P)l'(P)}{(l(P))^2}. \quad (70)$$

It is noticed that $l(P) > 0$ and $l'(P) > 0$ for $\forall P \in [0, +\infty)$. When $P \in [0, P^*)$, we have $g(P) > 0$ and $g'(P) < 0$, leading to the fact that $[f_{\text{EE}}(P)]'' < 0$, which means that $f_{\text{EE}}(P)$ is concave. While for the interval $P \in (P^*, +\infty)$, $[f_{\text{EE}}(P)]''$ can be either positive or negative, thus $f_{\text{EE}}(P)$ is only quasi-concave, and neither concave nor convex. In conclusion, $f_{\text{EE}}(P)$ is strictly increasing and concave at $[0, P^*)$ while strictly decreasing and only quasi-concave at $(P^*, +\infty)$. The proof is thus completed.

APPENDIX B PROOF OF PROPOSITION 1

First, when $P_T \leq P^*$, we know that $f_{\text{SE}}(P)$ is increasing at $[0, P_T] \in [0, P^*)$ given the fact that $f_{\text{SE}}(P)$ is strictly increasing with P . In addition, according to Lemma 2, we obtain that $f_{\text{EE}}(P)$ is also increasing at $[0, P_T]$. Thus, for $\forall P \in [0, P_T]$, we have $f_{\text{SE}}(P_T) > f_{\text{SE}}(P)$ and $f_{\text{EE}}(P_T) > f_{\text{EE}}(P)$, which results in $\mathcal{P} = \{P | P = P_T\}$.

Next, consider the case when $P_T > P^*$. As mentioned above, for $\forall P \in [0, P^*)$, we can always find a point P^* such that $f_{\text{SE}}(P^*) > f_{\text{SE}}(P)$ and $f_{\text{EE}}(P^*) > f_{\text{EE}}(P)$, which implies that $[0, P^*) \notin \mathcal{P}$. On the other hand, for $\forall P \in [P^*, P_T]$, there does not exist any other point P' such that both $f_{\text{SE}}(P') > f_{\text{SE}}(P)$ and $f_{\text{EE}}(P') > f_{\text{EE}}(P)$.

Therefore, $\mathcal{P} = \{P | P^* \leq P \leq P_T\}$. The proof is thus completed.

APPENDIX C PROOF OF LEMMA 3

First, $g_2(P)$ can be rewritten in eq. (28). It is noticed that the second and third terms of $g_2(P)$ is strictly decreasing with P . For the first term, let $A = \frac{\chi\zeta}{\ln 2}$, its first derivative can be given in eq. (29). For the molecule of eq. (29), since $\zeta > 0$, we therefore let

$$h(P) = (1 + A)\ln(1 + \zeta P) - \zeta P - \frac{\zeta AP}{1 + \zeta P}. \quad (71)$$

Furthermore, by defining $\rho = \zeta P$, so we have $\rho > 0$, and $h(\rho) = (1 + A)\ln(1 + \rho) - \rho - A\frac{\rho}{1 + \rho}$. The first derivative of $h(\rho)$ can be given as

$$h'(\rho) = \frac{1 + A}{1 + \rho} - 1 - \frac{A}{(1 + \rho)^2} = \frac{\rho[(A - 1) - \rho]}{(1 + \rho)^2}. \quad (72)$$

It is noticed that if $A \leq 1 + \rho$, which is a mild requirement in real environments, then $h'(\rho) < 0$, which means that $h(P)$ is decreasing with P . In addition, $\lim_{P \rightarrow 0^+} h(P) = 0$, so we can infer that when $P \in [0, +\infty)$, $h(P) \leq 0$. Therefore, we have $\left[\frac{\zeta P}{(1 + \zeta P + A)\ln(1 + \zeta P)} \right]' < 0$. Thus, the first term of $g_2(P)$ is also decreasing with P , so we achieve that $g_2(P)$ is strictly decreasing with P . The proof is thus completed.

REFERENCES

- [1] Y. Liu, *et al.*, “A survey of recent advances in optimization methods for wireless communications,” *IEEE J. Sel. Areas Commun.*, vol. 42, no. 11, pp. 2992-3031, 2024.
- [2] A. J. Paulraj, D. A. Gore, R. U. Nabar and H. Boleskei, “An overview of MIMO communications-a key to gigabit wireless,” *Proc. IEEE.*, vol. 92, no. 2, pp. 198-218, 2004.
- [3] S. Islam, N. Avazov, O. Dobre and K. Kwak, “Power-domain non-orthogonal multiple access (NOMA) in 5G systems: Potentials and challenges,” *IEEE Commun. Surv. Tut.*, vol. 19, no. 2, pp. 721-742, 2017.
- [4] E. Basar, “Noise modulation,” *IEEE Wireless Commun. Lett.*, vol. 13, no. 3, pp. 844-848, 2023.
- [5] Y. Liu, *et al.*, “Reconfigurable intelligent surfaces: Principles and opportunities,” *IEEE Commun. Surv. Tut.*, vol. 23, no. 3, pp. 1546-1577, 2021.
- [6] K. K. Wong, A. Shojaeifard, K. F. Tong and Y. Zhang, “Fluid antenna systems,” *IEEE Trans. Wireless Commun.*, vol. 20, no. 3, pp. 1950-1962, 2021.
- [7] L. Zhu, W. Ma and R. Zhang, “Modeling and performance analysis for movable antenna enabled wireless communications,” *IEEE Trans. Wireless Commun.*, vol. 23, no. 6, pp. 6234-6250, 2024.
- [8] S. Shan, C. Ouyang, Y. Li and Y. Liu, “Exploiting pinching-antenna systems in multicast communications,” *arXiv preprint arXiv:2506.00616*, 2025.
- [9] R. W. Heath, J. Carlson, N. V. Deshpande, M. R. Castellanos, M. Akroot and C. B. Chae, “The tri-hybrid MIMO architecture,” *arXiv preprint arXiv:2505.21971*, 2025.
- [10] Z. Ding, R. Schober and H. Vincent Poor, “Flexible-antenna systems: A pinching-antenna perspective,” *IEEE Trans. Commun.*, early access, 2025.
- [11] Y. Xu, Z. Ding and G. K. Karagiannidis, “Rate maximization for downlink pinching-antenna systems,” *IEEE Wireless Commun. Lett.*, vol. 14, no. 5, pp. 1431-1435, 2025.
- [12] A. Fukuda, H. Yamamoto, H. Okazaki, Y. Suzuki, and K. Kawai, “Pinching antenna: Using a dielectric waveguide as an antenna,” *NTT DOCOMO Tech. J.*, vol. 23, no. 3, pp. 5-12, 2022.
- [13] D. Tyrovolas, S. A. Tegos, P. D. Diamantoulakis, S. Ioannidis, C. K. Liaskos and G. K. Karagiannidis, “Performance analysis of pinching-antenna systems,” *IEEE Trans. Green Commun. Netw.*, early access, 2025.
- [14] C. Ouyang, Z. Wang, Y. Liu and Z. Ding, “Array gain for pinching-antenna systems (PASS),” *IEEE Commun. Lett.*, early access, 2025.
- [15] T. Hou, Y. Liu and A. Nallanathan, “On the performance of uplink pinching antenna systems (PASS),” *arXiv preprint arXiv:2502.12365*, 2025.
- [16] Z. Ding, H. V. Poor, “Analytical optimization for antenna placement in pinching-antenna systems,” *arXiv preprint arXiv:2507.13307*, 2025.
- [17] B. Zhang, H. Zhang, K. Yang, Y. Zhao and K. Wang, “On the performance analysis of pinching-antenna-enabled SWIPT systems,” *arXiv preprint arXiv:2509.03836*, 2025.
- [18] C. Ouyang, Z. Wang, Y. Liu and Z. Ding, “Rate region of ISAC for pinching-antenna systems,” *arXiv preprint arXiv:2505*, 2025.
- [19] Y. Cheng, C. Ouyang, Y. Liu and G. K. Karagiannidis, “On the performance of pinching-antenna systems (PASS) with orthogonal and non-orthogonal multiple access,” *arXiv preprint arXiv:2506.02420*, 2025.
- [20] Z. Zhou, Z. Yang, G. Chen and Z. Ding, “Sum-rate maximization for NOMA-assisted pinching-antenna systems,” *IEEE Wireless Commun. Lett.*, early access, 2025.
- [21] M. Zeng, J. Wang, X. Li, G. Wang, O. A. Dobre and Z. Ding, “Sum rate maximization for NOMA-assisted uplink pinching-antenna systems,” *arXiv preprint arXiv:2505.00549*, 2025.
- [22] S. Hu, R. Zhao, Y. Liao, D. W. Ng and J. Yuan, “Sum-rate maximization for pinching antenna-assisted NOMA systems with multiple dielectric waveguides,” *arXiv preprint arXiv:2503.10060*, 2025.
- [23] K. Wang, Z. Ding and R. Schober, “Antenna activation for NOMA assisted pinching-antenna systems,” *IEEE Wireless Commun. Lett.*, early access, 2025.
- [24] J. Zhang, H. Xu, C. Ouyang, Q. Zou and H. Yang, “Uplink sum rate maximization for pinching antenna-assisted multiuser MISO,” *arXiv preprint arXiv:2504.16577*, 2025.
- [25] Y. Li, J. Wang, M. Zeng and Y. Liu, “Sum rate maximization for wireless powered pinching-antenna systems (PASS),” *arXiv preprint arXiv:2506.00355*, 2025.
- [26] J. Zhao, X. Mu, K. Cai, Y. Zhu and Y. Liu, “Waveguide division multiple access for pinching-antenna systems (PASS),” *arXiv preprint arXiv:2502.17781*, 2025.
- [27] M. Zeng, X. Li, J. Wang, G. Huang, O. A. Dobre and Z. Ding, “Energy efficient resource allocation for NOMA-assisted uplink pinching-antenna systems,” *arXiv preprint arXiv:2505.07555*, 2025.
- [28] M. Zeng, J. Wang, G. Zhou, F. Fang and X. Wang, “Energy-efficient design for downlink pinching-antenna systems with QoS guarantee,” *arXiv preprint arXiv:2505.14904*, 2025.
- [29] G. Zhou, Y. Mao and B. Clerckx, “Rate-splitting multiple access for multi-antenna downlink communication systems: Spectral and energy efficiency tradeoff,” *IEEE Trans. Wireless Commun.*, vol. 21, no. 7, pp. 4816-4828, 2022.
- [30] Y. Liu, Z. Wang, X. Mu, C. Ouyang, X. Xu and Z. Ding, “Pinching-antenna systems (PASS): Architecture designs, opportunities, and outlook,” *arXiv preprint arXiv:2501.18409*, 2025.
- [31] A. Bereyhi, C. Ouyang, S. Asaad, Z. Ding and H. V. Poor, “MIMO-PASS: Uplink and downlink transmission via MIMO pinching-antenna systems,” *arXiv preprint arXiv:2503.03117*, 2025.
- [32] H. Al-Obiedullah, H. Bany Salameh and S. Abdel-Razeq, “Energy-spectral efficiency trade-off in IRS-assisted NOMA systems: A weighted product method,” *IEEE Trans. Green Commun. Netw.*, vol. 9, no. 2, pp. 635-644, 2025.
- [33] Z. Wang, C. Ouyang, X. Mu, Y. Liu and Z. Ding, “Modeling and beamforming optimization for pinching-antenna systems,” *arXiv preprint arXiv:2502.05917*, 2025.
- [34] J. Zhao, H. Song, X. Mu, K. Cai, Y. Zhu and Y. Liu, “Pinching-antenna systems-enabled multi-user communications: transmission structures and beamforming optimization,” *arXiv preprint arXiv:2508.14458*, 2025.
- [35] Y. Liu, Q. Luo, G. Chen, *et al.*, “Joint Beamforming and Position Optimization for Fluid STAR-RIS-NOMA Assisted Wireless Communication Systems,” *arXiv preprint arXiv:2507.06904*, 2025.